Acta Cryst. (1980). B36, 2881–2890

Charge Density in Anhydrite, $CaSO_4$, from X-ray and Neutron Diffraction Measurements

BY A. KIRFEL AND G. WILL

Mineralogisches Institut der Universität Bonn, Lehrstuhl für Mineralogie und Kristallographie, Poppelsdorfer Schloss, D-5300 Bonn, Federal Republic of Germany

(*Received* 12 *May* 1980; *accepted* 13 *August* 1980)

Abstract

The room-temperature electron-density distribution in natural anhydrite, $CaSO_4$, has been studied by both X-ray and neutron diffraction. Conventional refinements of the data sets yielded $R_w^X = 0{\cdot}020$ and $R_w^N = 0{\cdot}025$. The X-ray intensities were also used for high-order refinements, a refinement based on a point-charge model for the representation of positive residual charge accumulations, and a multipole expansion refinement. All these refinements were performed to study and to reduce parameter bias arising from bonding effects. The multipole expansion model yielded the significantly improved $R_w = 0{\cdot}0116$. The resulting $(X-X)$ and $(X-N)$ dynamic deformation density maps showed features qualitatively in agreement. Special attention was given to the charge distribution within and around the $[SO_4]^{2-}$ anion. The observed bond density distribution is different from earlier results obtained from comparable sulfate derivatives and from the $[S_2O_6]^{2-}$ anion, indicating a considerable $3d$ population of the S atom.

Introduction

Anhydrite, $CaSO_4$, is one of the principal sulfate minerals. The crystal structure was investigated by Wasastjerna (1925) and by Dickinson & Binks (1926). Later work by Cheng & Zussman (1963), who adopted the lattice constants determined by Swanson, Fuyat & Ugrinic (1955) and those of Höhne (1961, 1962), confirmed the structure proposed by Wasastjerna. Recent single-crystal X-ray diffraction studies were reported by Morikawa, Minato, Tomita & Iwai (1975) and by Hawthorne & Ferguson (1975), who obtained $R = 0{\cdot}021$ (266 reflections, $s_{max} = 0{\cdot}807$ Å^{-1}) and 0·016 (284 reflections, $s_{max} = 0{\cdot}756$ Å^{-1}) respectively.

The crystal structure of $CaSO_4$ can be regarded as well established. Apart from different orientations used for the unit cell there are no discrepancies. The standard setting is *Cmcm*; however, Hawthorne & Ferguson (1975) pointed out that the setting *Amma* is preferable for showing the relations between anhydrite and its hydrates, and we have therefore also adopted this orientation for the present study. The aim of this was to extend the range of the scattering angle in order to evaluate the bonding electron-density distribution, *i.e.* the deviations of $\rho(\mathbf{r})$ from the spherical free-atom model produced by chemical bonding.

Our specific interest is directed towards the $[SO_4]^{2-}$ anion. In an earlier study of the bonding in $[S_2O_6]^{2-}$ of $Na_2S_2O_6.2H_2O$ and its deuterated homologue (Kirfel & Will, 1980) we found significant dynamic and static deformation densities of the atomic electron shells due to dominant covalent bonding contributions in the S—O and S—S bonds. In that case it was possible to corroborate the twofold negative-charge character of the anion within the limits of tolerance, and to conclude that the deviations of the atoms from neutrality are smaller than assumed earlier from chemical considerations. For anhydrite we anticipated finding correspondingly interesting results for the electron distribution in and around the anion. In this paper we report the results obtained from both X-ray and neutron diffraction measurements. Besides the conventional refinement procedure we have also used the multipole expansion refinement technique (Hirshfeld, 1971; Harel & Hirshfeld, 1975), which leads to a description of the static deformation density distribution. We have found this technique to be also applicable to second-row elements such as S in $[S_2O_6]^{2-}$ (Kirfel & Will, 1980). Numerical results of this latter refinement, including standard crystallographic parameters and related results, are given here without further comment. A detailed description of the multipole refinement process and the resulting static deformation density distribution requires more extensive consideration, and will therefore be reported in a subsequent paper.

Experimental

The anhydrite investigated was a natural mineral specimen from Stassfurt, Federal Republic of Germany, taken from the Institute's museum. The chemical

0567-7408/80/122881-10$01.00

composition of this mineral is very close to stoichiometric (Flörke, 1952) with an impurity content negligible for X-ray and neutron diffraction experiments: Na_2O, K_2O 0·02 wt%; SrO 0·01 wt%; Al_2O_3, Fe_2O_3 0·04 wt%.

(*a*) *X-ray measurements*

The crystal selected for the X-ray diffraction measurements was of irregular shape with dimensions between 0·08 and 0·12 mm. Attempts to grind a spherical sample failed due to the known cleavage behavior of $CaSO_4$. Data were collected on an automatic four-circle diffractometer (Syntex $P2_1$) with Mo $K\alpha$ radiation (λ = 0·71069 Å) from a graphite monochromator ($2\theta_m$ = 12·2°). The cell parameters were determined by least squares from the angular settings of 25 independent reflections. The intensity measurements were carried out in the θ–2θ scan mode with a 2° plus (α_1,α_2) dispersion scan range. The scan speed was adjusted between 1·0 and 10·0° min^{-1}, and the total background time equalled the time spent at the peak count. Six standard reflections were remeasured after every 28 scans. The intensities of these did not vary to any significant degree. A complete half of the sphere was scanned up to a maximum of 2θ = 100° (sin θ/λ = 1·078 Å^{-1}), leading to 3369 recorded reflections (omitting standards). In the data reduction the intensities were normalized according to the fluctuations of the sums of the check-reflection intensities. Symmetry-related reflections were then averaged, resulting in a set of 801 unique reflections of which 186 were regarded as unobserved ($I < 3\sigma$). The internal agreement index of the data based on the deviations of the $|F_{\mathbf{h},i}|$ of equivalent reflections from their mean values $|\bar{F}_{\mathbf{h}}|$ was

$$R_f = \sum_{\mathbf{h}} \sum_{i} \big||\bar{F}_{\mathbf{h}}| - |F_{\mathbf{h},i}|\big| / \sum_{\mathbf{h}} \sum_{i} |F_{\mathbf{h},i}| = 0{\cdot}029.$$

An estimate of the absorption effect (μ = 2·33 mm^{-1}) yielded transmissions in the range of 79·5 ± 3·5% corresponding to maximum errors in the structure amplitudes of 2·2%. Owing to the irregular shape of the sample no absorption corrections were applied. The crystallographic data and the information on the data collection and processing are summarized in Tables 1 and 2.

Table 1. *Crystallographic data*

	MMTI*	HF†	This work
a_0 (Å)	6·992 (1)	6·993 (2)	7·006 (1)
b_0 (Å)	6·999 (1)	6·995 (2)	6·998 (1)
c_0 (Å)	6·240 (1)	6·245 (1)	6·245 (1)
V (Å^3)			306·2 (1)
Space group	*Bmmb*	*Amma*	*Amma*
M_r			136·138
Z	4	4	4
D_x (Mg m^{-3})			2·952
μ(Mo $K\alpha$) (mm^{-1})			2·33

* MMTI: Morikawa, Minato, Tomita & Iwai (1975).
† HF: Hawthorne & Ferguson (1975).

Table 2. *Data collection*

	X-ray	Neutron
Wavelength (Å)	0·71069	0·8418
Crystal dimensions (mm)	0·08–0·12	0·8 × 0·9 × 1·0
Maximum θ (°)	50	58
(sin $\theta/\lambda)_{max}$ (Å^{-1})	1·078	1·01
Scan mode	θ–2θ step scan	θ–2θ step scan
Scan angle (°)	2 plus (α_1,α_2)	variable
Number of steps/reflection	96	35
Scan speed (° min^{-1})	1·0–10·0	
Monitor count		70 000
Number of check reflections	6	3
Check reflection interval	28	50
Number of reflections recorded	3369	2028
Number of unique reflections	801	720
Number of unobserved reflections	186 ($I < 3\sigma$)	117 ($F^2 < 2{\cdot}5\sigma$)
Internal match R_f	0·029	0·032

(*b*) *Neutron measurements*

The neutron diffraction measurements were performed at the high-flux reactor facilities of the Institut Laue–Langevin, Grenoble, France. The crystal selected for the experiment was 0·8 × 0·9 × 1·0 mm. The lattice constants obtained from the X-ray measurements were used to refine the neutron wavelength from the adjusted angular settings of 14 independent reflections (λ = 0·8418 Å). The intensity measurements were then carried out in the θ–2θ scan mode on the four-circle diffractometer D9 with a monitor rate of 70 000 counts. Each scan consisted of 35 steps, 5 steps of 0·15° for the background on each side, and 25 peak steps of variable step length. The total scan range was calculated from the known resolution curve of the instrument. Three standard reflections were remeasured after every 50 scans. 2028 reflections were recorded (omitting standards), the maximum 2θ being 116° (sin θ/λ = 1·01 Å^{-1}). The data reduction for the individual measurements was performed at ILL with the College V system employing the minimal $\sigma(I)/I$ method for the net-intensity evaluation (Lehmann & Larsen, 1973; Lehmann, 1975; Zwoll, 1974). Equivalent reflections were then averaged, resulting in 720 unique reflections, of which 117 were regarded as unobserved ($F^2 < 2{\cdot}5\sigma$). The internal agreement index defined as for the X-ray data was R_f = 0·032. A measurement of the linear absorption coefficient was performed on the University of Bonn four-circle diffractometer NANCY (Zwoll, Müller & Will, 1976) at the DIDO research reactor, Kernforschungsanlage Jülich, Federal Republic of Germany, with a crystal plate of 4 mm thickness.

With a neutron wavelength of 1·203 Å, μ was determined as 0·0243 mm^{-1}. According to the BNL cross-section compilation (*Neutron Cross Sections*, 1976) the absorption is about the same at 0·84 Å, which was the wavelength for the diffraction measurements, and therefore no correction was considered necessary.

Structure refinements

(*a*) *Conventional refinements*

(i) The conventional all-data refinement was by full-matrix least squares starting with the positional parameters given by Hawthorne & Ferguson (1975). For the X-ray data, scattering factors for Ca^{2+}, S and O were taken from *International Tables for X-ray Crystallography* (1974). The reflections were weighted with their own σ's [$w = 1/\sigma^2(F)$] and an isotropic extinction correction (Zachariasen, 1963), $F_{corr} = kF_o[1 + \beta(2\theta)gI_o]$, was taken into account by including g in the list of variables. The final value of g was 6×10^{-6}, leading to a maximum correction factor of 1·116 for the 020 reflection. Refinement was stopped when the calculated parameter shifts were well below one-tenth of the associated e.s.d.'s. The final $R_{overall} = 0{\cdot}032$ and $R_w = 0{\cdot}022$ (0·020 in each case when unobserved reflections were omitted). The goodness-of-fit (GOF) was 1·22.

(ii) In order to reduce possible bias of the standard atomic parameters arising from bonding effects, high-order refinements were also carried out, these being referred to as HO1 ($\sin\theta/\lambda > 0{\cdot}7$ Å^{-1}), HO2 ($\sin\theta/\lambda > 0{\cdot}8$ Å^{-1}) and HO3 ($\sin\theta/\lambda > 0{\cdot}9$ Å^{-1}). In all cases an extinction correction was found to be unnecessary. As in similar investigations the resulting high-order scale factors were smaller than the scale factor obtained from the conventional all-data refinement. The scale factors, agreement indices, number of observations used, and GOF figures are listed in Table 3.

(iii) In an ensuing conventional refinement of the X-ray data, referred to as the bond model (BM) (compare also Kirfel & Will, 1980), residual density accumulations observed in the foregoing (X–N) syntheses were represented by point scatterers $E(1)$ to $E(7)$ ($f = 1{\cdot}0$) with multiplicities, positional parameters and anisotropic thermal parameters as variables. The aim of this refinement was (*a*) to check for a significant model improvement and (*b*) to detect whether the charge clouds can be considered to describe the bonding effects, and thus reduce the bias of the atomic parameters. To minimize correlation problems the refinement was performed by adjusting the parameters in subsequent cycles as follows: scale factor, atomic positions, atomic vibrations, E multiplicities, E positions and E vibrations. The parameter shifts were reduced to 0·1 of the calculated shifts at the beginning, this constraint being released to 0·5 in the final stage. The results related to the BM refinement are summarized in Tables 3 to 8 together with the other refinement results.*

(iv) Refinement of the neutron diffraction data was also based on their own σ's. The scattering lengths $b(Ca) = 0{\cdot}47$, $b(S) = 0{\cdot}28$, and $b(O) = 0{\cdot}58 \times 10^{-14}$ m were taken from Bacon (1977). Owing to considerable correlation between the scale factor and the isotropic extinction coefficient, the scale factor and the positional parameters were refined in one cycle, the vibrational parameters and the extinction coefficient in the next. The final maximum extinction correction factor was 1·037 for the 600 reflection. The refinement was stopped at $R_{overall} = 0{\cdot}046$ and $R_w = 0{\cdot}027$ (0·034 and 0·025 respectively when unobserved reflections were omitted). A preliminary refinement, with a scattering length for Ca of $0{\cdot}49 \times 10^{-14}$ m taken from *International Tables for X-ray Crystallography* (1974), yielded vibrational parameters u_{ij} for Ca which were unreasonably large ($u_{11} = 0{\cdot}0075$, $u_{22} = 0{\cdot}0102$, and $u_{33} = 0{\cdot}0074$ Å^2). A comparison with Table 5 demonstrates the importance of using the proper scattering length.

(*b*) *Multipole expansion refinement*

The multipole expansion model (Hirshfeld, 1971; Harel & Hirshfeld, 1975) used in the refinement of

* Lists of structure factors for X-ray and neutron diffraction data have been deposited with the British Library Lending Division as Supplementary Publication No. SUP 35515 (13 pp.). Copies may be obtained through The Executive Secretary, International Union of Crystallography, 5 Abbey Square, Chester CH1 2HU, England.

Table 3. *Structure refinements of the X-ray and neutron diffraction data*

	All data	HO1	HO2	HO3	BM	MM	Neutron
$\sin\theta/\lambda$ range (Å^{-1})	0·0–1·08	0·7–1·08	0·8–1·08	0·9–1·08	0·0–1·08	0·0–1·08	0·0–1·01
Number of reflections	801	549	428	276	801	801	720
Scale factor	0·649 (1)	0·648 (3)	0·643 (6)	0·647 (16)	0·642 (1)	0·658 (1)	2·077 (2)
$R_{overall}$	0·032	0·042	0·050	0·058	0·028	0·028	0·046
R_0 (omitting unobserved)	0·020	0·020	0·022	0·021	0·016	0·0156	0·034
R_w	0·022	0·023	0·027	0·033	0·015	0·0147	0·027
R_w (omitting unobserved)	0·020	0·016	0·017	0·018	0·0125	0·0116	0·025
Goodness-of-fit	1·22	0·78	0·79	0·80	0·84	1·01	0·67

X-ray diffraction data expresses the charge density of a stationary atomic arrangement by a superposition of spherical free-atom densities, defined by the input scattering curves, together with a deformation density which is approximated by linear combinations of localized deformation functions (see also Kirfel, Gupta & Will, 1979; Kirfel & Will, 1980). The adjustment of all sets of deformation functions is carried out by variation of the multipole coefficients, which are usually given initial values of zero. The radial distribution of the deformation functions, described by a parameter α for each deformation type, may also be varied. After completion of the all-data refinement the final sets of deformation functions are believed to describe static deformation densities of the spherical free atoms due to bonding. If the multipole expansion leads to a significant improvement in the agreement, the standard crystallographic parameters can be expected to be less biased by bonding effects. This applies especially for the vibrational parameters, for which case the separation of the aspherical valence electron distribution is highly desirable.

In the present study the site symmetries are *mm* for Ca and S and *m* for each of the two crystallographically different O atoms. The sets of deformation functions to be assigned must be compatible with these site symmetries, leading to a complete set of multipoles with 110 non-vanishing members, of which 64 are independently adjustable. In order to reduce the problem of correlations, which can be serious owing to the redundancy of the analytical electron-density description, a first refinement (*MULT*1) was performed with alternating cycles for the standard crystallographic parameters and the multipole coefficients. A refinement with strongly reduced parameter shifts was found useful at the beginning. When all parameters tended to converge towards a level of stability, the α values were released and refined in intermittent cycles. This procedure is time-consuming; however, inspection of the parameter changes showed that the refinement process was steady, no parameter oscillations being observed. As in the previous refinements extinction was taken into account by separate variation of an isotropic extinction factor *g*. The maximum correction was 1·105 for the 020 reflection, in good agreement with the conventional refinement. After 67 cycles $R_{overall} = 0{\cdot}028$ and $R_w = 0{\cdot}0147$ (0·0156 and 0·0116 respectively omitting unobserveds). The GOF was 1·01.

A second refinement, referred to as *MULT*2, was performed under the same conditions, except that the atomic parameters, positional and vibrational, were taken from the neutron data refinement and kept constant throughout the multipole refinement procedure. If one regards the neutron parameters as the true ones, the adjustment of the deformation functions should describe the $(X-N)$ density. *MULT*2 was stopped at $R_{overall} = 0{\cdot}031$ and $R_w = 0{\cdot}0165$ (0·0185 and 0·0138 respectively omitting unobserveds). Since the atomic parameters were not affected, the results are not included in the tables. A detailed discussion and a comparison of the *MULT*1 and *MULT*2 deformation density results will be reported separately. The agreement factors obtained with both multipole refinements indicate a significant improvement in the description of the observed electron density, compared to the conventional refinement results.

Refinement results

The agreement indices and other information related to the different refinements are listed in Table 3. The refined scale factors vary between 0·642 and 0·658, corresponding to a model-dependent uncertainty $\Delta(k)/k$ of about 1·25%. For the ensuing difference-density calculations the mean value $k = 0{\cdot}6478$ was regarded as the most reliable measure. Table 4 contains the positional parameters of the atomic sites in the crystallographic setting *Amma*: Ca^{2+} $\frac{3}{4},0,z$; S $\frac{1}{4},0,z$; O(1) $\frac{1}{4},y,z$; and O(2) $x,0,z$. The positional parameters derived from the X-ray measurements describe the positions of the centers of (i) three-dimensional Gaussian electron distribution functions (symmetry *mmm*) in conventional refinements, and (ii) electron distribution functions of the atomic-site symmetries in the multipole expansion refinement, both adjusted to minimize deviations of the observed density. If we take the positions of the nuclei determined from the neutron diffraction measurements as reference points, then the former positions may give information about bonding effects on the electron shells.

(i) Significant differences, exceeding the associated sums of the e.s.d.'s, say, are only found for z[O(1)]. These, however, tend to become smaller with increasing cut-off angle (HO refinements) and for the bond model. This finding indicates a polarization of the O(1) electron shell along $\mathbf{c}_0$ towards the Ca^{2+} cation.

(ii) This polarization becomes even clearer from the multipole refinement, where we observe a significant shift of 0·0065 Å of O(1) in comparison to the neutron results. The important features of this shift are: (*a*) the direction, which is towards the symmetry-equivalent O(1); (*b*) it is parallel within 5° to the O(1)—Ca bond line. In addition, the multipole refinement reveals some polarization of the S atom towards Ca^{2+} (shift 0·0025 Å). Since we do not find a comparable polarization for O(2), we may conclude that the $[SO_4]^{2-}$ anion as a whole is polarized, and possesses a dipole moment parallel to [001] and pointing towards Ca (z = 0·65235). This is corroborated by comparing the z coordinates of the centers of gravity of SO_4 for the various refinements: all-data 0·15624 (13), HO1 0·15627 (15), HO2 0·15629 (20), HO3 0·15619 (29),

Table 4. *Positional parameters* ($\times 10^5$) *with e.s.d.'s in parentheses*

The atomic sites are Ca^{2+} $\frac{3}{4},0,\bar{z}$; S $\frac{1}{4},0,z$; O(1) $\frac{1}{4},y,z$; O(2) $x,0,z$.

		All data	HO1	HO2	HO3	BM	MM	Neutron
Ca^{2+}	z	−34761 (7)	−34762 (7)	−34761 (9)	−34761 (14)	−34765 (4)	−34763 (5)	−34765 (11)
S	z	15564 (8)	15562 (9)	15566 (12)	15563 (19)	15567 (5)	15537 (5)	15577 (17)
O(1)	y	16954 (14)	16957 (17)	16952 (20)	16918 (31)	16973 (10)	16906 (10)	16956 (7)
	z	1549 (14)	1567 (18)	1574 (22)	1563 (32)	1584 (11)	1520 (12)	1607 (7)
O(2)	x	8171 (14)	8179 (14)	8205 (18)	8203 (25)	8186 (9)	8196 (10)	8202 (7)
	z	29760 (16)	29754 (20)	29746 (26)	29732 (35)	29747 (11)	29752 (12)	19735 (7)

Table 5. *Vibrational parameters* ($\times 10^4$ Å^2) *with e.s.d.'s in parentheses*

		All data	HO1	HO2	HO3	BM	MM	Neutron
Ca^{2+}	u_{11}	63 (1)	63 (1)	61 (2)	62 (4)	66 (1)	61 (1)	68 (2)
	u_{22}	94 (1)	94 (1)	93 (2)	94 (4)	94 (1)	92 (1)	95 (2)
	u_{33}	68 (1)	68 (1)	66 (2)	69 (4)	65 (1)	66 (1)	68 (2)
S	u_{11}	63 (2)	64 (2)	64 (2)	67 (4)	60 (1)	65 (1)	59 (3)
	u_{22}	69 (2)	68 (2)	67 (2)	68 (4)	66 (1)	63 (1)	69 (3)
	u_{33}	60 (2)	57 (1)	55 (2)	53 (4)	56 (1)	51 (1)	47 (3)
O(1)	u_{11}	183 (4)	187 (3)	191 (5)	191 (7)	185 (3)	182 (3)	178 (2)
	u_{22}	87 (3)	87 (3)	83 (3)	88 (5)	85 (2)	81 (2)	84 (1)
	u_{33}	105 (3)	97 (3)	96 (4)	96 (5)	98 (2)	95 (2)	90 (1)
	u_{23}	27 (3)	28 (2)	27 (3)	29 (4)	27 (2)	31 (2)	24 (1)
O(2)	u_{11}	68 (4)	68 (4)	65 (5)	72 (5)	66 (2)	65 (2)	64 (1)
	u_{22}	176 (4)	178 (3)	180 (5)	180 (7)	179 (3)	174 (3)	173 (2)
	u_{33}	108 (3)	107 (3)	105 (3)	100 (5)	104 (2)	102 (2)	91 (1)
	u_{13}	20 (3)	18 (2)	17 (3)	16 (4)	18 (2)	20 (2)	15 (1)

BM 0·15633 (9), MM 0·15603 (10), and neutron 0·15640 (10). Based on the MM results, the shift of the electron distribution center of gravity towards Ca^{2+} is 0·0023 (14) Å with respect to the nuclei. The resultant dipole moment can therefore be estimated as p = 0·11 (7) e Å, or 1·7 (1·0) $\times 10^{-30}$ Cm (water molecule 6·3 $\times 10^{-30}$ Cm). This is, however, only an indication since the associated e.s.d. is of the same magnitude. A polarization of the Ca^{2+} cation could not be detected.

The question arises, which of the X-ray data refinements leads to the best positional parameters, *i.e.* which ones deviate least from the nuclear positions, and are therefore best suited for $(X-X)$ deformation density calculations. This can be answered by considering the r.m.s. discrepancies (p^X–p^N) as a statistical criterion. Since the three lattice constants are rather similar, the calculation can be applied to the fractional coordinates. This yields the sequence ($\times 10^5$): all data 29·3, HO1 21·6, HO2 15·1, HO3 24·3, BM 14·8, and MM 44·5. Hence, the HO2 and BM results are closest to the neutron results with average displacements reduced to only 0·001 Å. The large MM discrepancy is due to the observed polarization of O(1) and S.

Finally, a comparison of the atomic positions from the conventional X-ray data refinement with the latest published positions (Morikawa, Minato, Tomita & Iwai, 1975; Hawthorne & Ferguson, 1975) does not show significant differences. The anisotropic vibrational parameters u_{ij} (Å^2) are listed in Table 5. In general, the results obtained from both X-ray and neutron diffraction are in reasonable agreement. Table 6 contains the values $B_{eq} = 8\pi^2\bar{u}$ (Å^2) with corresponding values from the above authors for comparison. Again, taking the nuclear vibrations as reference points the following features can be observed from Tables 5 and 6:

(i) On average, the electron-shell vibrational parameters tend to be larger than the corresponding nuclear parameters. This is understandable assuming that the former still contain to some extent deformations of the electron shells due to covalent bonding. The stable Ca^{2+} electron configuration is not expected to be significantly affected by bonding. Scheringer, Kutoglu & Mullen (1978) have pointed out that vibrational parameters obtained from room-temperature neutron diffraction measurements, which are not corrected for TDS, are usually smaller than those determined from X-ray data. Hence, smaller nuclear vibrations compared to the electron-shell vibrations can be explained partially by a lack of the

Table 6. *Equivalent isotropic temperature factors* B_{eq} (Å^2) *and r.m.s. discrepancies* $(u_{ij}^X - u_{ij}^N)$ ($\times 10^4$ Å^2)

$B_{eq} = 8\pi^2 \bar{u}$.

	All data	HO1	HO2	HO3	BM	MM	Neutron	HF*	MMTI†
Ca^{2+}	0·59 (1)	0·59 (1)	0·58 (2)	0·59 (3)	0·59 (1)	0·58 (1)	0·61 (2)	0·65	0·72
S	0·51 (2)	0·50 (1)	0·49 (2)	0·49 (3)	0·48 (1)	0·47 (1)	0·46 (2)	0·55	0·64
O(1)	0·99 (3)	0·98 (2)	0·97 (3)	0·98 (4)	0·97 (2)	0·94 (2)	0·93 (1)	0·99	1·06
O(2)	0·93 (3)	0·93 (3)	0·92 (3)	0·93 (4)	0·92 (2)	0·90 (2)	0·86 (1)	0·94	1·03
R.m.s.d.	8·1	7·0	7·1	6·8	6·0	5·2			

* HF: Hawthorne & Ferguson (1975).
† MMTI: Morikawa, Minato, Tomita & Iwai (1975).

Table 7. *Rigid-bond test: mutual atomic vibrations* $z^2_{A,B}$ *and* $z^2_{B,A}$ ($\times 10^4$ Å^2)

	All data		HO1		HO2		HO3		BM		MM		Neutron	
S–O(1)	66	67	64	64	63	68	63	63	62	64	59	54	61	64
S–O(2)	62	63	62	64	61	63	62	66	59	63	60	59	54	59
O(1)–O(2)	100	101	96	102	96	101	96	101	97	101	88	96	93	93
R.m.s. (SO_4)	1·9		3·6		3·2		3·7		3·5		5·5		3·3	
S–Ca	60	68	57	68	55	66	53	69	56	65	51	66	47	68

TDS correction. However, such differences should then be found for all atoms, which is contradicted by the Ca atom vibrations. We may therefore conclude that TDS is not a dominant factor in the observed differences in the vibration tensors.

(ii) If we look at the sequence of the cut-off angles of the HO refinements and the sophistication of the models applied for refinement we find that the X-ray results gradually approach the nuclear vibration values. This indicates that an improved separation between thermal vibrations and deformation of the electron shell induced by bonding has been achieved. This becomes especially clear by following the changes in the u_{33} parameters of the O and S atoms. One can therefore expect significant bond density features along [001].

A statistical comparison of the X-ray parameter sets with the nuclear vibrations in terms of r.m.s. discrepancies is shown in Table 6. The results from the multipole expansion refinement are clearly the most favorable for $(X–X)$ syntheses. The r.m.s. value of 5·2 $\times 10^{-4}$ Å^2 is only about 1·5 times the sum of the mean e.s.d.'s of the u_{ij} considered.

A check for the physical significance of the refined vibrational parameters of the SO_4 group atoms was also performed by a rigid-bond test (Hirshfeld, 1976). Results are given in Table 7. All r.m.s. discrepancies are of the order of two to three times $\sigma(u_{ij})$.

Structural results

Detailed descriptions of the structure of anhydrite have been given in earlier structure determinations and it suffices here to summarize the main structural features briefly. The structure is built up of chains of alternating SO_4 tetrahedra and CaO_8 dodecahedra, running along [001]. Thus each S atom (point symmetry *mm*) is coordinated by four O atoms with two unique S–O bonds, and each Ca^{2+} cation (*mm*) is coordinated by eight O atoms with four unique Ca–O distances (Fig. 1). While the SO_4 tetrahedron is almost regular [deviations Δ(S–O) < 0·003 Å], the CaO_8 dodecahedron is considerably distorted with strongly contracted edges shared with the SO_4 groups. The Ca–S distances are almost equal within the chain, 3·102 (1) and 3·143 (1) Å, adding up to the lattice constant c_0 = 6·245 (2) Å. The above discussed dipole moment is directed along the shorter Ca–S distance. Selected interatomic distances and bond angles are given in Table 8. The distances and angles exhibit no significant differences between X-ray (conventional refinements) and neutron results except for a small shortening of the S–O(2) bond and an opening of the associated O(2)–S–O(2) angle subtended by edges shared with the Ca polyhedron. Such an opening implies an asymmetric bond density distribution with respect to the S–O(2) bond directions, *i.e.* some charge accumulation inside the angle. From the positional parameters of the multipole expansion refinement we find a reversed situation for the S–O bonds. Here, S–O(1) is 0·003 Å shorter than S–O(2). In addition the tetrahedral bond angles are contracted by 0·33° for the O(1)–S–O(1) angle and by 0·23° for O(2)–S–O(2) compared to the neutron results. This finding is a consequence of the above mentioned shifts of the

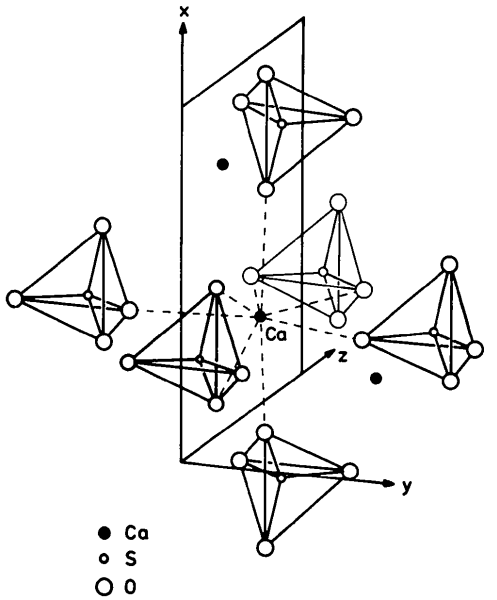

Fig. 1. Schematic drawing of the crystal structure of $CaSO_4$. Octahedral coordination of Ca cation by $[SO_4]^{2-}$ anions.

electron-shell centers of gravity of O(1) and S compared to their nuclear positions as revealed by the application of the adjustable multipole functions.

Dynamic deformation densities from *X–X* and *X–N* syntheses

The dynamic deformation density distribution in $CaSO_4$ was investigated by calculation of difference maps ($s \leq 0{\cdot}80$ Å)

$$\Delta\rho(\mathbf{r}) = \frac{2}{V}\sum_{\mathbf{h}}\left(\frac{1}{\kappa}|F_{\mathbf{h}}^{\mathrm{obs}}| - |F_{\mathbf{h}}^{\mathrm{calc}}|\right)\cos\left[2\pi(\mathbf{hr} + \alpha_{\mathbf{h}})\right].$$

The structure factors $F_{\mathbf{h}}^{\mathrm{calc}}$ were computed from the parameters derived from : (*a*) the X-ray high-order data refinement HO1 (Figs. 2*a*, 3*a*); (*b*) the refinements BM (positional) and MM (vibrational) (Figs. 2*b*, 3*b*); and (*c*) the neutron data refinement (Figs. 2*c*, 3*c*, 3*d*). The ensuing $\Delta\rho$ syntheses yielded therefore (*X–X*) (*a* and *b*) and (*X–N*) (*c* and *d*) maps. The scale factor was taken as $k = 0{\cdot}6478$ in all cases. Since all atoms occupy special positions, it suffices to calculate three sections, namely the mirror planes (010) at $y = 0$ and (100) at $x = 0{\cdot}25$ (both containing S and Ca simultaneously), and the general section through O(1)–S–O(2). The first sections show the bond-angle plane O(2)–S–O(2) (Fig. 2*a*,*b*,*c*), the second ones O(1)–S–O(1) (Fig. 3*a*,*b*,*c*), and Fig. 3(*d*) shows the (*X–N*) density in the general section. As to be expected from the discussion of parameters, we observe increasingly pronounced residual density features in the order (*a*) to (*c*). Qualitatively, however, there are no significant differences between the maps, *e.g.* all corresponding maps reproduce the main features of the deformation density almost equally well. It is worthwhile noting that the syntheses (*b*) and (*c*) yielded almost identical results, except in the vicinities of the atomic positions, which are generally associated with large uncertainties. This indicates that most of the information contained in the (*X–N*) maps could be evaluated from the application of the different refinement models to the X-ray data alone. Although this point cannot be generalized at present, it certainly deserves further attention.

The general appearance of the deformation density distributions in the O–S–O planes is different from earlier results of similar atomic arrangements of sulfate derivatives like sulfamic acid (Bats, Coppens & Koetzle, 1977), Na sulfanilate (Bats, 1977), and Na

Table 8. *Selected bond distances* (Å) *and angles* (°) *with e.s.d.'s in parentheses*

	All data	BM	MM	Neutron
SO_4 tetrahedron				
S–O(1)	1·474 (1)	1·474 (1)	1·472 (1)	1·473 (1)
S–O(2)	1·475 (1)	1·474 (1)	1·475 (1)	1·472 (1)
⟨S–O⟩	1·4745 (7)	1·4740 (7)	1·4735 (7)	1·4725 (7)
O(1)–O(1^{i})	2·373 (1)	2·376 (1)	2·366 (1)	2·373 (1)
O(1)–O(2)	2·429 (1)	2·427 (1)	2·428 (1)	2·424 (1)
O(2)–O(2^{xi})	2·358 (1)	2·356 (1)	2·355 (1)	2·354 (1)
O(1)–S–O(1^{i})	107·16 (6)	107·35 (5)	107·01 (5)	107·34 (7)
O(1)–S–O(2)	110·90 (3)	110·85 (2)	110·98 (2)	110·84 (1)
O(2)–S–O(2^{xi})	106·12 (6)	106·13 (5)	105·96 (5)	106·19 (7)
⟨O–S–O⟩	109·48 (4)	109·48 (3)	109·48 (3)	109·48 (3)
CaO_8 dodecahedron				
Ca–O(1^{vi})	2·466 (1)	2·463 (1)	2·469 (1)	2·464 (1)
Ca–O(1)	2·559 (1)	2·562 (1)	2·556 (1)	2·563 (1)
Ca–O(2^{ii})	2·345 (1)	2·346 (1)	2·347 (1)	2·347 (0)
Ca–O(2^{iii})	2·510 (1)	2·510 (1)	2·509 (1)	2·510 (1)
O(1)–O(1^{vii})	3·319 (1)	3·318 (1)	3·322 (1)	3·319 (1)
O(1)–O(2^{ii})	3·261 (1)	3·263 (1)	3·259 (1)	3·263 (1)
O(1)–O(2^{viii})	3·480 (1)	3·479 (1)	3·484 (1)	3·481 (1)
O(1)–O(2^{vi})	2·931 (1)	2·931 (1)	2·932 (1)	2·932 (1)
O(2)–O(2^{iv})	2·775 (1)	2·777 (1)	2·777 (1)	2·780 (1)
O(1)–Ca–O(1^{i})	55·24 (3)	55·24 (2)	55·14 (2)	55·17 (2)
O(1^{v})–Ca–O(1^{ii})	82·67 (3)	82·63 (2)	82·73 (2)	82·62 (2)
O(2^{ii})–Ca–O(1^{ix})	92·65 (1)	92·65 (1)	92·65 (1)	92·65 (1)
O(2^{ii})–Ca–O(2^{iii})	69·63 (3)	69·68 (3)	69·68 (3)	69·73 (2)
O(2^{ii})–Ca–O(1)	83·22 (2)	83·20 (2)	83·21 (2)	83·19 (2)
O(2^{v})–Ca–O(1^{iii})	72·18 (3)	72·21 (2)	72·16 (2)	72·24 (2)
O(2^{iii})–Ca–O(2^{x})	56·04 (3)	55·99 (2)	55·96 (2)	55·92 (2)
Ca–S^{iii}	3·102 (1)	3·102 (0)	3·104 (0)	3·101 (1)
Ca–S	3·143 (1)	3·143 (0)	3·141 (1)	3·144 (1)
Ca–S^{vi}	3·499 (1)	3·499 (1)	3·499 (1)	3·499 (1)

Symmetry code

(i) $x,-y,z$
(ii) $-x,-y,-z$
(iii) $x,y,z-1$
(iv) $-x,-y,1-z$
(v) $x,\frac{1}{2}-y,\frac{1}{2}-z$
(vi) $x,\frac{1}{2}+y,z-\frac{1}{2}$
(vii) $x,\frac{1}{2}-y,\frac{1}{2}+z$
(viii) $-x,\frac{1}{2}-y,\frac{1}{2}-z$
(ix) $x,y-\frac{1}{2},z-\frac{1}{2}$
(x) $\frac{1}{2}-x,y,z-1$
(xi) $\frac{1}{2}-x,y,z$

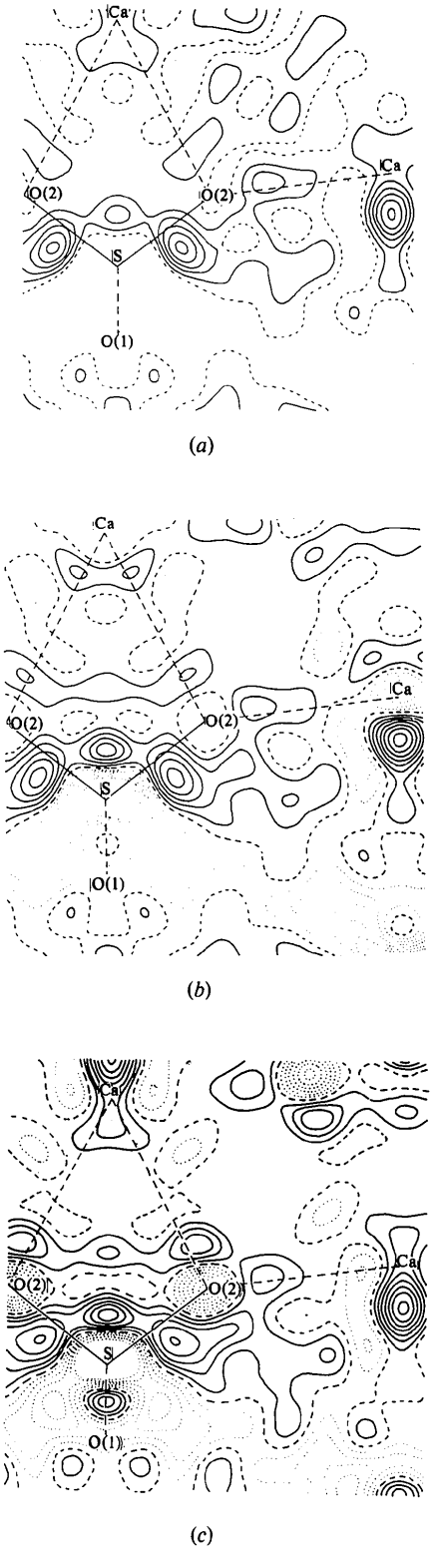

Fig. 2. Dynamic deformation density distribution in the mirror plane (010) at $y = 0$. Levels at 0·1 e Å^{-3}, zero line broken, negative contours dotted. (*a*) (*X*–*X*) parameters from HO1 refinement; (*b*) (*X*–*X*) parameters from BM (positional) and MM (vibrational) refinements; (*c*) (*X*–*N*).

dithionate (Kirfel & Will, 1980). In these cases distinct features of the bonding were σ-bond charge accumulations of almost cylindrical symmetry about the S–O bonds, clearly separated by a region of negative deformation density along the bisectrix of the O–S–O bond angle. From the qualitative agreement of these findings one could be led to expect that the density distribution within the SO_4 tetrahedron is characteristic for this atomic arrangement, and is hardly affected by external bonding conditions. The present study implies that this is not true in all cases.

(i) In Fig. 2, which depicts the mirror plane containing the O(2)–S–O(2) bond angle, we observe a considerable deviation of the σ-bond overlap from the straight S–O(2) connection. A peak >0·50 e Å^{-3} is shifted towards the crossing of the imaginary lines connecting Ca–O(2) and Ca–S. A plausible explanation for this shift can be based on Coulomb attraction forces exerted by the adjacent Ca^{2+} cations. Another reason can be found in the repulsion from the charge accumulation, which we observe on the bisectrix of the O(2)–S–O(2) bond angle. This peak may be associated with interaction of the $3d_z$ orbital of S with the $2p$ orbitals of the O(2) atoms according to the π-bond model (Cruickshank, 1961) designed to explain the shortness of the S–O bonds in sulfates and related derivatives. There is also a charge accumulation on the O(2)–Ca connecting line, obviously belonging to O(2). This peak and the symmetry-related one are also connected by a band of positive deformation density with a small maximum in the middle. Compared to the situation around O(1) discussed below we observe an additional peak on the short O(2)–Ca connecting line [2·354 (1) Å], which is approximately normal to c_0 and provides bonding between adjacent Ca···SO_4···Ca chains running along [001]. The lack of cylindrical symmetry of the S–O(2) bond density can also be observed from a section through the middle of the bond normal to the bond direction (Fig. 4*a*).

(ii) The mirror plane containing O(1)–S–O(1) is depicted in Fig. 3. The peak height of the σ-bond charge accumulation is 0·44 e Å^{-3}. In this case the peak maximum is slightly shifted towards the bisectrix of the O(1)–S–O(1) bond angle. As in Fig. 2 the two S–O(1) bond peaks are not completely separated but connected by a band of almost uniform positive density (~0·30 e Å^{-3}) (Fig. 3*c*). Fig. 4(*b*) shows the density distribution normal to the S–O(1) bond direction. As in Fig. 4(*a*) the peak shift and the asymmetry of the σ-bond charge accumulation are clearly visible. Considerable charge accumulation of the order of 0·40 e Å^{-3} is also observable along the O(1)–Ca connecting line, showing that the lone-pair electrons of O(1) are involved in bonding to the cation. Here, too, there is a bridging band, although of lower density, between the two equivalent O(1)–Ca peaks. The finding of density accumulations outside the anion localized between the

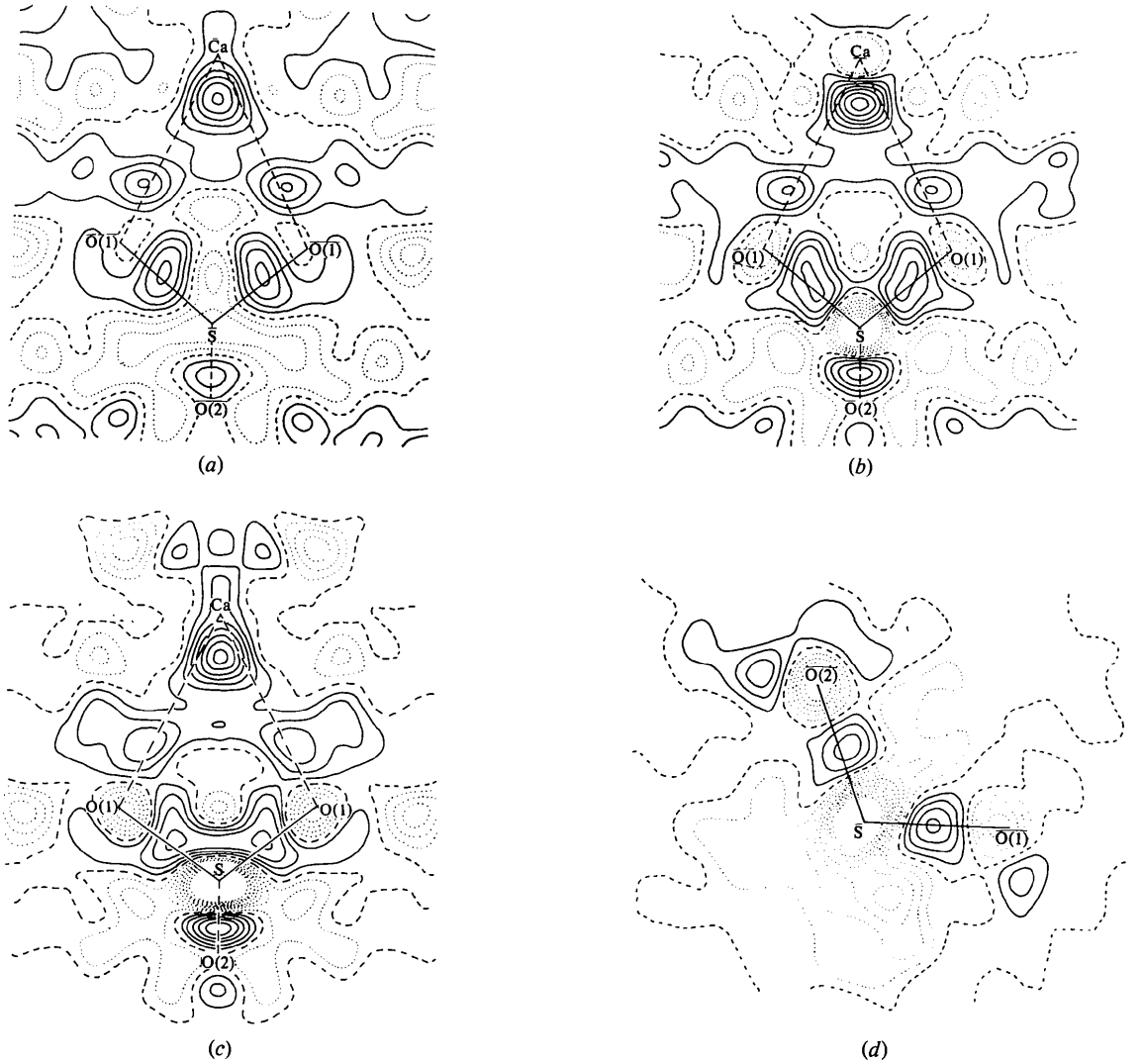

Fig. 3. Dynamic deformation density distribution in the mirror plane (100) at $x = \frac{1}{4}$. (*a*) to (*c*) as in Fig. 2. (*d*) (*X–N*) difference density in the plane through O(1), S, O(2).

cation and both the O(2) and O(1) atoms indicates an interaction between the SO_4 group and the Ca^{2+} ion, which is not of a purely ionic nature.

(iii) Fig. 3(*d*) shows the (*X–N*) residual density distribution in the section defined by O(1)–S–O(2). Contrary to the bond angles in the mirror planes, this general section displays the above mentioned separation of σ-bond peaks by a region of negative deformation density. Thus, in a first approximation the charge redistribution within the SO_4 tetrahedron due to bonding leads to concentrations in two sorts of banana-shaped regions perpendicular to each other and clearly separated by negatively charged surroundings. This result is definitely different from that in Na dithionate, where well-resolved sp^3 hybrid lobes around the S atoms could be observed.

(iv) Close to the Ca position, on the longer of the two Ca–S distances, which sum to c_0, there is a peak $>0{\cdot}70$ e Å^{-3}. Although difference-density features in the vicinity of an atom position are not very reliable, the peak indicates a polarization of the closed electron shell of the cation towards the O(1)–S–O(1) bond angle. Such a polarization can be understood as being due to the electric field exerted by the above mentioned dipole moment of the SO_4 group, and hence is supporting evidence for its existence.

(v) The features described for the deformation density are shown as *ORTEP* plots (Johnson, 1965) in Fig. 5(*a*) and (*b*), produced from the parameters of the BM refinement. The simple, open 50% probability ellipsoids represent the positions and the three-dimensional Gaussian distributions of the point charges refined to describe the positive deformation densities in the maps of Figs. 2 and 3. In particular, the deviations of the S–O bond charges from the straight S–O connecting lines (*E*1 and *E*4), the peak on the

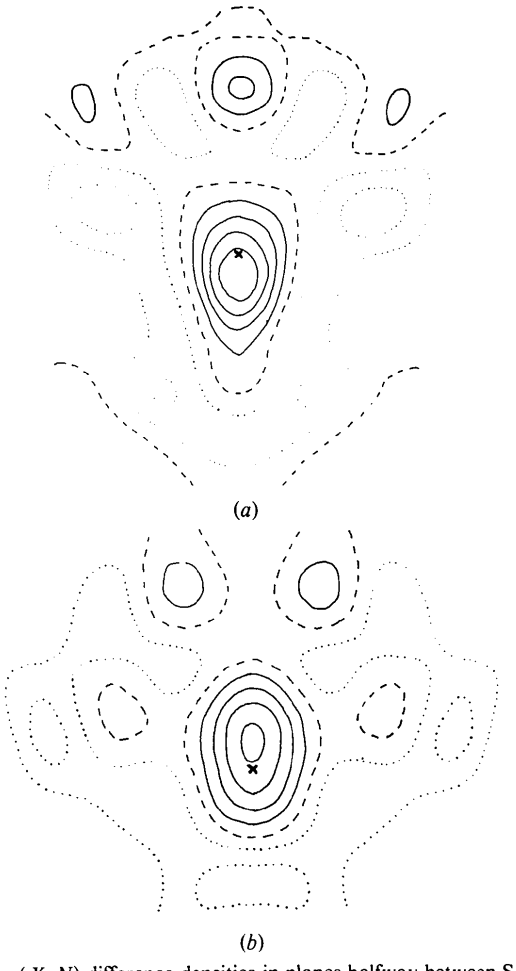

Fig. 4. (X–N) difference densities in planes halfway between S and O atoms and normal to the S–O bonds. Levels at 0·1 e Å^{-3}, zero line broken, negative contours dotted. (*a*) S–O(2); (*b*) S–O(1).

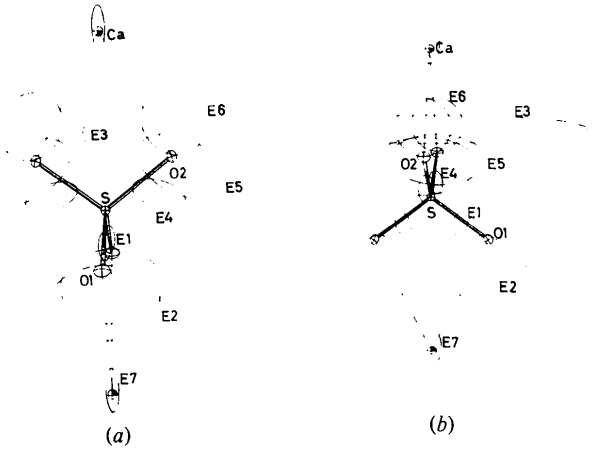

Fig. 5. *ORTEP* plots of the charge cloud distribution in and around the $[SO_4]^{2-}$ anion of $CaSO_4$ derived from the bond-model refinement. The atoms are represented by their refined vibration tensors. The arrangement is approximately viewed along (*a*) [010] and (*b*) [100].

O(2)–S–O(2) bisectrix ($E3$) and the asymmetric charge distribution at Ca^{2+} ($E7$) are clearly reproduced.

This work has received support from the Deutsche Forschungsgemeinschaft which is gratefully acknowledged. The authors are also indebted to R. Feld and M. S. Lehmann (Institut Laue–Langevin, Grenoble) for their help with the neutron data collection. Finally, we thank I. Christidis (University of Thessaloniki) for his help with some of the calculations during a fellowship stay at Bonn.

References

BACON, G. E. (1977). *Neutron Diffraction Newsletter* 1977. Neutron Diffraction Communication of the International Union of Crystallography.

BATS, J. W. (1977). *Acta Cryst.* B**33**, 2035–2041.

BATS, J. W., COPPENS, P. & KOETZLE, T. F. (1977). *Acta Cryst.* B**33**, 37–45.

CHENG, G. C. H. & ZUSSMAN, J. (1963). *Acta Cryst.* **16**, 767–769.

CRUICKSHANK, D. W. J. (1961). *J. Chem. Soc.* pp. 5486–5504.

DICKINSON, E. C. & BINKS, W. (1926). *Philos. Mag.* **2**, 114–128.

FLÖRKE, O. W. (1952). *Neues Jahrb. Mineral. Abh.* **84**, 189–240.

HAREL, M. & HIRSHFELD, F. L. (1975). *Acta Cryst.* B**31**, 162–172.

HAWTHORNE, F. C. & FERGUSON, R. B. (1975). *Can. Mineral.* **13**, 289–292.

HIRSHFELD, F. L. (1971). *Acta Cryst.* B**27**, 769–781.

HIRSHFELD, F. L. (1976). *Acta Cryst.* A**32**, 239–244.

HÖHNE, E. (1961). *Fortschr. Mineral.* **39**, 374–383.

HÖHNE, E. (1962). *Monatsber. Dtsch. Akad. Wiss. Berlin*, **4**, 72–77.

International Tables for X-ray Crystallography (1974). Vol. IV. Birmingham: Kynoch Press.

JOHNSON, C. K. (1965). *ORTEP*. Report ORNL-3794. Oak Ridge National Laboratory, Tennessee.

KIRFEL, A., GUPTA, A. & WILL, G. (1979). *Acta Cryst.* B**35**, 2291–2300.

KIRFEL, A. & WILL, G. (1980). *Acta Cryst.* B**36**, 512–523.

LEHMANN, M. S. (1975). *J. Appl. Cryst.* **8**, 619–622.

LEHMANN, M. S. & LARSEN, F. K. (1974). *Acta Cryst.* A**30**, 580–584.

MORIKAWA, H., MINATO, I., TOMITA, T. & IWAI, S. (1975). *Acta Cryst.* B**31**, 2164–2165.

Neutron Cross Sections (1976). 3rd ed., Vol. 2, BNL-325. National Neutron Cross Section Center, Brookhaven.

SCHERINGER, C., KUTOGLU, A. & MULLEN, D. (1978). *Acta Cryst.* A**34**, 481–483.

SWANSON, H. E., FUYAT, R. K. & UGRINIC, G. M. (1955). *Natl Bur. Stand. (US) Circ.* **539**, 65–67.

WASASTJERNA, J. A. (1925). *Soc. Sci. Fenn. Commentat. Phys. Math.* **2**, 26.

ZACHARIASEN, W. H. (1963). *Acta Cryst.* **16**, 1139–1144.

ZWOLL, K. (1974). *Ber. Kernforschungsanlage Jülich*, No 1057.

ZWOLL, K., MÜLLER, K. D. & WILL, G. (1976). *Kerntechnik*, **10**, 435–441.